AIP Applied Physics Letters

Observation of the intrinsic Gilbert damping constant in Co/Ni multilayers independent of the stack number with perpendicular anisotropy

Hyon-Seok Song, Kyeong-Dong Lee, Jeong-Woo Sohn, See-Hun Yang, Stuart S. P. Parkin et al.

Citation: Appl. Phys. Lett. **102**, 102401 (2013); doi: 10.1063/1.4795013
View online: http://dx.doi.org/10.1063/1.4795013
View Table of Contents: http://apl.aip.org/resource/1/APPLAB/v102/i10
Published by the American Institute of Physics.

APPLIED PHYSICS LETTERS **102**, 102401 (2013)

Observation of the intrinsic Gilbert damping constant in Co/Ni multilayers independent of the stack number with perpendicular anisotropy

Hyon-Seok Song,[1] Kyeong-Dong Lee,[1] Jeong-Woo Sohn,[1,2] See-Hun Yang,[3] Stuart S. P. Parkin,[3] Chun-Yeol You,[4] and Sung-Chul Shin[1,2,a)]
[1]*Department of Physics and Center for Nanospinics of Spintronic Materials, Korea Advanced Institute of Science and Technology, Daejeon 305-701, South Korea*
[2]*Department of Emerging Materials Science, DGIST, Daegu 711-873, South Korea*
[3]*IBM Research Division, Almaden Research Center, San Jose, California 95120, USA*
[4]*Department of Physics, Inha University, Incheon 402-751, South Korea*

(Received 26 September 2012; accepted 26 February 2013; published online 11 March 2013)

We investigate the intrinsic Gilbert damping constant in perpendicular magnetic anisotropy Co/Ni multilayer system by means of an all-optical method. We find that the intrinsic Gilbert damping constant does not depend on the stack number and the perpendicular magnetic anisotropy when the magnetic field is high enough. In contrast, the extrinsic Gilbert damping is strongly correlated with the inhomogeneous anisotropy distribution in the low-field regime, as observed in magneto-optical images. Intriguingly, the extrinsic Gilbert damping is consistently reduced with decreasing length scale in the measurements, providing a concrete means to determine the intrinsic Gilbert damping. © *2013 American Institute of Physics*. [http://dx.doi.org/10.1063/1.4795013]

Perpendicular magnetic anisotropy (PMA) architectures are desired to improve memory density and to overcome the thermal stability problems in spin-transfer torque magnetic random access memory. The PMA architecture typically has a smaller switching current density J_c because it is free from demagnetization fields. However, PMA materials typically have larger Gilbert damping constants than typical in-plane ferromagnetic materials, leading to larger values of J_c because J_c is proportional to the Gilbert damping constant α.[1] Therefore, the determination of the Gilbert damping constant of PMA materials is important. Furthermore, it is widely accepted that α is closely related to the spin-orbit interaction,[2,3] which is also a main source of PMA. Therefore, the relationship between the Gilbert damping and PMA has been widely investigated. Recently, this connection has been supported by many research groups for various PMA systems, such as Pt/Co/Pt (Ref. 4) and $[Co/Pd]_8$.[5] In contrast, other groups have reported that there are no correlations between the Gilbert damping and PMA in $Co_{90}Fe_{10}$/Ni,[6] $Co_{90}Fe_{10}$/Pd,[7] Co/Pt,[8] and Ta-buffered Co/Ni (Ref. 9) multilayer systems.

In another aspect, the determination of the intrinsic α in a multilayer system is controversial. Generally, it is believed that α value increases with an increase in the stack number N due to the plausible increase of the roughness and defects with an increase in the number of interfaces.[8] However, some recent reports have shown that α is independent of N (Ref. 9) or inversely correlated to N.[10] Hence, the understanding of α mechanism remains incomplete, especially in multilayer system with different numbers of stacks.

Furthermore, the precise determination of α is an elaborate process that depends on the samples and the measurement techniques. Usually in real samples, spin waves are additionally generated from the non-magnetic or magnetic inhomogeneity such as the roughness, defects, the unsaturated magnetization state, or the anisotropy distribution. Therefore, the measured α includes not only the intrinsic α but also extrinsic α from the additional spin wave contribution, such as the apparent dephasing of various excited spin-wave precession frequencies and the additional direct and indirect relaxation via the interaction among the spin waves. The apparent dephasing is easily excluded by applying a strong enough external magnetic field because the strong magnetic field aligns the spins in one direction and reduces the incoherent precessional motion coming from the inhomogeneous anisotropy and demagnetization field distribution.[11] Interestingly, the extent of the incoherent precessional motion can also be reduced with decreasing length scale in the measurement.

In this letter, we studied α in $[Co/Ni]_N$ multilayer system, which have a low switching current and strong thermal stability,[12] while systematically controlling PMA with changing N from 6 to 27. In this sample system, we measured α as a function of both N and PMA by using an all-optical method. To identify the apparent effect, we investigated α by varying the external magnetic field H. Intriguingly, it was also found that the all-optical measurement technique with decreasing beam size can reduce the long-range inhomogeneity effect remarkably.

The Co/Ni multilayer films were prepared on a Si/SiO_2 (001) substrate by DC magnetron sputtering with a base pressure of 5×10^{-9} Torr. The stack structure of the sample series is $Si/SiO_2/Al_2O_3$(100 Å)/Ti(50 Å)/Co(3 Å)/[Ni(7 Å)/Co(3 Å)]$_N$/TaN(50 Å). We changed N as follows: increase by three consecutively from 6 to 27. We used a polar magneto-optical Kerr effect (p-MOKE), a vibration sample magnetometer (VSM), and a superconducting quantum interference device (SQUID) to measure the magnetic properties of the samples. Figure 1(a) shows the hysteresis loops measured by p-MOKE at room temperature. By utilizing the in-plane VSM and SQUID, the effective PMA energy density K_{eff} is estimated from $K_{eff} = M_s H_s/2$, where M_s is the saturation magnetization and H_s is the saturation magnetic field in the

a)Electronic addresses: shin@kaist.ac.kr and scshin@dgist.ac.kr.

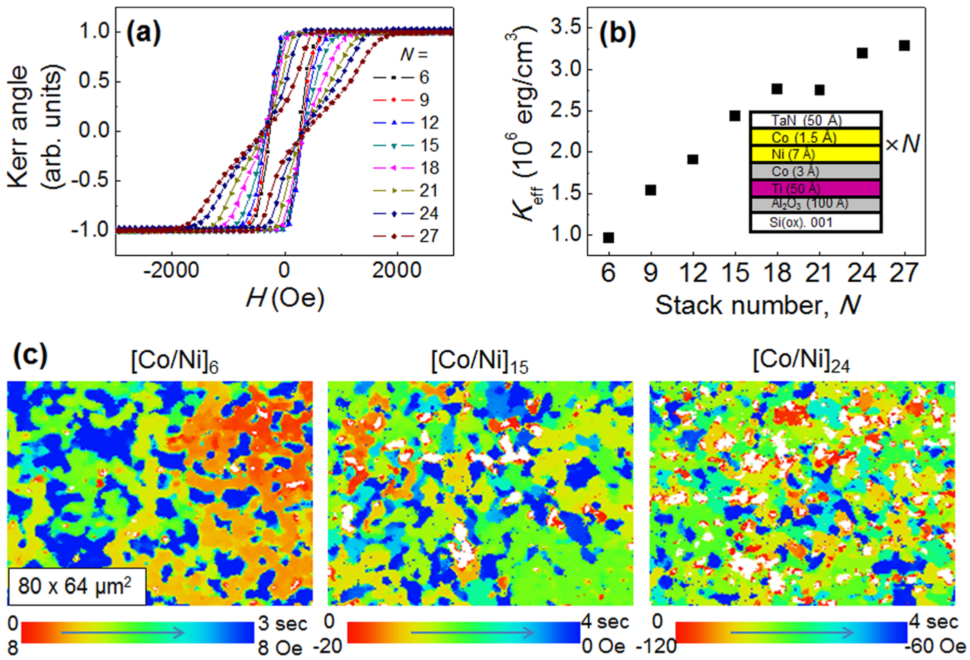

FIG. 1. (a) The magnetic hysteresis loop measurement by p-MOKE. (b) Anisotropy as a function of the multilayer stack number N. The inset shows the structure of the Co/Ni multilayer films. (c) Field-swept domain reversal patterns measured using a magneto-optical microscope magnetometer at $N = 6$, 15, and 24. White color represents the unreversed area.

film plane. The K_{eff} value is plotted as a function of N in Fig. 1(b). In general, the K_{eff} increases as the N increases. Because magnetic inhomogeneity is an important issue in the PMA samples, we also investigated the magnetic inhomogeneity using a magneto-optical microscope magnetometer (MOMM).[13,14] Field-swept domain reversal patterns are visualized from the initial saturated state with $N = 6$, 15, and 24 in Fig. 1(c). This figure shows the domain reversal pattern in color codes with the field sweeping rates of 0, 5, and 15 Oe/s near the coercive field. As N increases, the field-swept domain reversal pattern becomes more nucleation-dominant which indicates increased anisotropy-distribution.[15] Also, the sweeping field range increases concomitantly, which implies growth of local coercivity distribution or ΔH_c by the accumulation of the number of stacks.[13]

Measurements of α were carried out by using time-resolved MOKE.[16] A Kerr-lens mode-locked Ti:Sapphire oscillator generates laser pulses with a center wavelength of ~800 nm. The laser pulse has a pulse width of 30 fs and a repetition rate of 82 MHz. We doubled the frequency of the probe beam used here with a BBO crystal; thus, the laser beam is split into a pump beam and a probe beam. The probe beam intensity is much weaker than that of the pump beam (1:200). The pump and probe laser pulses are fed into a 50× (0.5 numerical aperture) polarization-conserving objective lens, as shown in Fig. 2(a). The probe beam is incident along the normal axis of the sample. The spot diameters of the pump and probe beams are ~2 μm and ~1 μm, respectively. The pump fluence F is in the range of 4–20 mJ/cm^2. To check thermal effect from the pump beam, we measured dynamic Kerr loops with $N = 6$ at $F = 8$ mJ/cm^2 (not shown here). We found out that the transient heating and cooling is negligible unless the experimental error really matters. In addition, compared the loop between with and without the pump beam, we estimated that the sample was heated up to ~360 K. This result is in good agreement with the previous report.[17] To reduce the noise, we used balanced detection and lock-in amplifier filtering via mechanical chopping on the pump beam at 1300 Hz. The external magnetic field was applied with the angle θ_H of 60° from the normal direction of the film plane.

Figure 2(b) shows the time-resolved MOKE data with $N = 6$–27 at $H = 5.0$ kOe, $\theta_H = 60°$, and $F = 8$ mJ/cm^2. In the Kerr signals, the step-like decrease at 2 ps reflects the demagnetization, and the damped harmonic oscillation after a few ps reflects the precessional motion.[18] The Kerr signals are fitted to a damped-harmonic function expressed as

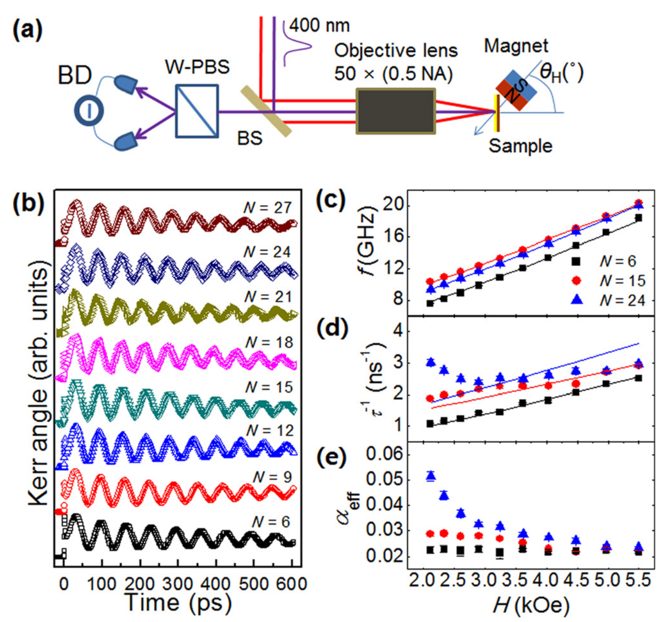

FIG. 2. (a) A schematic of the experimental setup (BS: beam splitter; W-PBS: Wollaston polarizing beam splitter; BD: balanced detector). (b) Time-resolved Kerr signals (open symbols) and fitting curves (solid curves) with [Co/Ni]$_N$ multilayer films of $N = 6$–27. Experimental data (solid symbols) and fitting curves (solid curves) of (c) the resonance frequency f, (d) the inverse of the relaxation time τ^{-1}, and (e) the effective damping constant α_{eff} as a function of the external magnet field H when $\theta_H = 60°$. Note that the size of the error bar in (a) is similar to that of the data symbol.

TABLE I. Fitted and extracted values obtained in Co/Ni multilayer films when $N = 6$, 15, and 24. The $H_{K_1}^{\mathrm{eff}}$ values are determined by VSM and SQUID measurements while the other values are obtained by the fitting procedure.

N	$H_{K_1}^{\mathrm{eff}}$ (Oe)	H_{K_2} (Oe)	γ (Mrad/s Oe)	$g = \gamma\hbar/\mu_B$
6	1080	0 ± 570	20.9 ± 0.7	2.38 ± 0.08
15	4200	2350 ± 100	19.0 ± 0.2	2.16 ± 0.02
24	5790	4220 ± 40	18.8 ± 1.3	2.14 ± 0.14

$\theta = \theta_0 + Ae^{-t/t_0} + Be^{-t/\tau}\sin(2\pi ft + \varphi)$,[19] where the first term θ_0 represents the offset background, the second term is the remagnetization with relaxation time t_0, and the final term is the precessional motion with the resonance frequency f, the relaxation time τ, and the initial phase φ. The solid curves in Fig. 2(b) are the fitted lines.

Figure 2(c) shows f as a function of H with $N = 6$, 15, and 24. Here, $\theta_H = 60°$ and $F = 12\,\mathrm{mJ/cm^2}$. In this figure, the value of f increases as H increases. In order to understand this tendency, we fitted the data with the Kittel equation, as shown by the solid curves in Fig. 2(c). In the samples with a large N, the polar hysteresis loops in Fig. 1(a) do not show a sharp square shape. This suggests that the second-order anisotropy K_2 exists, and the K_2 value increases as the total Co thickness increases.[20] Therefore, we consider the following Kittel equation with K_2: $f = (\gamma/2\pi)\sqrt{H_1H_2}$, where $H_1 = H\cos(\theta_H - \theta) + H_{K_1}^{\mathrm{eff}}\cos^2\theta - H_{K_2}\cos^4\theta$ and $H_2 = H\cos(\theta_H - \theta) + H_{K_1}^{\mathrm{eff}}\cos 2\theta + H_{K_2}(3\cos^2\theta\sin^2\theta - \cos^4\theta)$. Here γ is the gyromagnetic ratio defined as $\gamma = g\mu_B/\hbar$. The equilibrium angle θ is calculated using the energy equilibrium relationship of $\sin 2\theta = 2H/H_{K_1}^{\mathrm{eff}}\sin(\theta_H - \theta) + (H_{K_2}/H_{K_1}^{\mathrm{eff}})\cos^2\theta\sin\theta$, where $H_{K_1}^{\mathrm{eff}} = 2K_{u1}/M_s + 4K_{u2}/M_s - 4\pi M_s$ and $H_{K_2} = 4K_{u2}/M_s$.[19] We used the $H_{K_1}^{\mathrm{eff}}$ value from the experimental data measured by the in-plane VSM and SQUID. By considering H_{K_2}, we obtained fairly well-matched fitting curves, as shown in Fig. 2(c). As expected, the fitted H_{K_2} values increase notably as N increases. We obtained g values that were close to the g value of bulk Co. The final best fit values of γ and H_{K_2} are summarized in Table I.

With these fitting parameters, we first estimated the possible single effective damping constant of α_{fit} by fitting the experimental data of τ^{-1} as a function of H when $\tau^{-1} = \gamma\alpha_{\mathrm{fit}}/2\ (H_1 + H_2)$. The estimated single damping constants are 0.024 ± 0.001, 0.026 ± 0.002, and 0.031 ± 0.005 for $N = 6$, 15, and 24, respectively. The value of α_{fit} increases slightly with increasing N, and the corresponding error also increases. For $N = 6$ shown with the black square symbols in Fig. 2(d), the experimental values of τ^{-1} are well fitted to the τ^{-1} curve using a single instance of α_{fit}. However, as N becomes large, the fitted curves deviate more from the experimental data in the small-field regime. Therefore, the error ranges are very large, and the α_{fit} values are far from intrinsic value. Silva *et al.*[6] showed that α is well-described by the weighted average of the individual contributions of α from the various atomic species in $Co_{90}Fe_{10}$/Ni multilayers and alloys. Concretely, by using bulk values, Silva *et al.* calculated α_{ave} and reported that α_{ave} is in excellent agreement with the experimental data. We calculate α_{ave} in our Co/Ni multilayers by using the same method and the values of bulk α_{Co} and α_{Ni}.[21] The estimated α_{ave} value is $\sim$0.22, which is well matched with the α_{fit} value of $N = 6$.

Figure 2(e) shows the experimental effective damping parameter α_{eff} as a function of H. The value of α_{eff} is obtained from the simple approximate equation of $\alpha_{\mathrm{eff}} = (2\pi f\tau)^{-1}$ using the experimental data of f and τ in Fig. 3.[22,23] Here, α_{eff} accounts not only for the intrinsic α but also for the extrinsic damping such as spin pumping and additional spin wave contribution. Therefore, the intrinsic α is smaller than the α_{eff} values.[11,19] The value of α_{eff} decreases as the external field increases in Fig. 2(e). Because the effective damping changes as the applied H is varied, the change in α_{eff} originates from the additional spin-wave damping or the apparent effect of the incoherent spin waves, which easily arise in samples with an inhomogeneous anisotropy distribution in a low H.[11,24] This explains why the variation of α_{eff} for $N = 24$ is larger than that for $N = 6$ because the inhomogeneity of K_{eff} for $N = 24$ is larger than that for $N = 6$, as shown in Fig. 1(c). Clearly, the α_{eff} values converge to the nearly identical minimum values under a high external magnetic field irrespective of the stack number $N = 6$, 15, and 24. This value is similar to $\sim$0.22 obtained by α_{ave}.

As described in the supplementary material,[25] we checked the effect of magnetization tilted angle on α, for example, by short wavelength spin waves. However, in our samples, the influence of short wavelength spin waves on damping is less operative when H is strong enough, which is well matched with the previous report.[22]

To analyze this in more detail with respect to N as well as K_{eff}, we measure α_{eff} under weak and strong H for various N. Figure 3(a) shows the α_{eff} dependences on N at 3.2 kOe and 5.0 kOe when $\theta_H = 60°$. When H is not strong enough (3.2 kOe), α_{eff} increases as N increases noticeably after $N = 9$. However, α_{eff} shows nearly a constant value with increasing N at sufficiently high external magnetic fields.

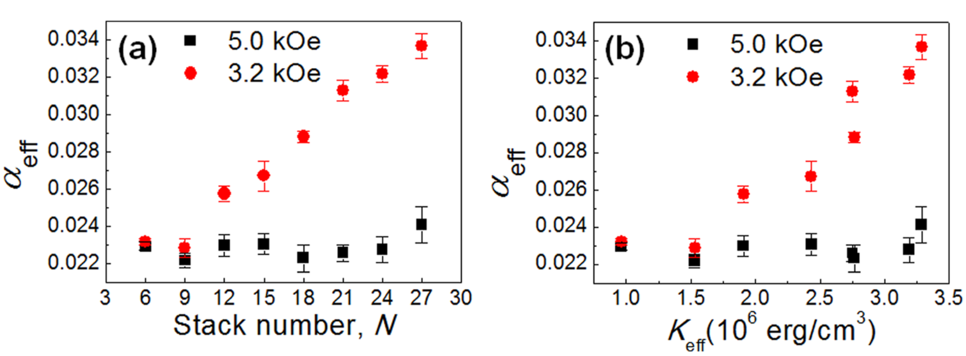

FIG. 3. (a) The dependence of α_{eff} on the stack number N and (b) the effective PMA energy density K_{eff}. Red and black solid circles represent the data of the low external magnet field $H = 3.2$ kOe and the high external magnet field $H = 5.0$ kOe, respectively.

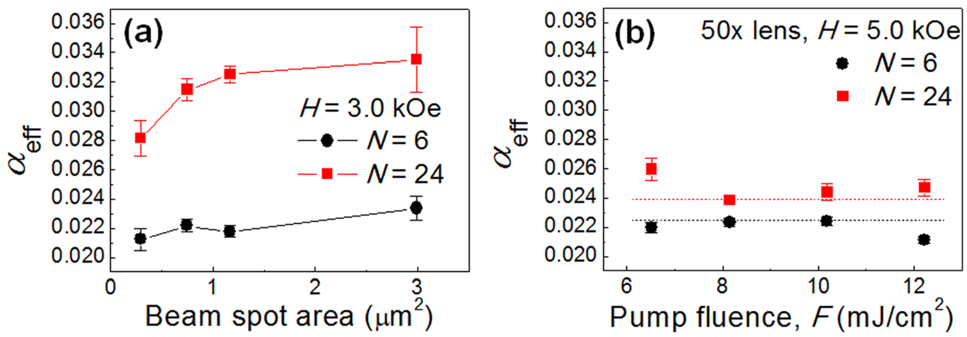

FIG. 4. (a) Effective Gilbert damping constant α_{eff} as a function of the probe beam spot area with various degrees of magnification by an objective lens at 10×, 20×, 50×, and 100× when $H = 3$ kOe at $\theta_H = 60°$. (b) The value of α_{eff} as a function of the pump fluence F. The black and red dashed lines are visual guide lines whose values are obtained from Fig. 2(e) with $H = 5.5$ kOe.

Therefore, our result shows that the intrinsic α is indeed independent of N from 6 to 27 within the experimental error. This calls attention to the other possible relationships between the PMA and the Gilbert damping.

To elucidate the relationship between the PMA and α_{eff}, we plot α_{eff} as a function of K_{eff}, as shown in Fig. 3(b). The value of α_{eff} increases rapidly when the anisotropy field level is exceeds the external magnetic field. However, the value of α_{eff} is independent of K_{eff} under a high external magnetic field. This means that the intrinsic α is independent of K_{eff} in our Ti-buffered Co/Ni multilayer system.

To verify the inhomogeneity effect at low field in another way, we first carried out experiments by varying the magnification of the objective lenses at 10×, 20×, 50×, and 100× with numerical apertures of 0.25, 0.4, 0.5, and 0.95, respectively. Figure 4(a) shows the value of α_{eff} as a function of the probe beam spot area. We used a pump power of 20 mW, in the front of the objective lens and a weak external magnetic field of $H = 3.0$ kOe at $\theta_H = 60°$. Compared to the result of $H = 3.0$ kOe, similar but weak trend (not shown here) is obtained in a strong external magnetic field of $H = 5.0$ kOe. Surprisingly, we noted an increasing relation between α_{eff} and the probe beam area. Since varying the magnification changes not only the probe area but also F in our experimental configuration, we also checked α_{eff} while varying the pump fluence with fixed magnification of 50× lens. As shown in Fig. 4(b), F has no clear relationship to α_{eff}. In addition, α_{eff} with $N = 24$ was significantly decreased compare to that of $N = 6$. This means that the probe beam area influences the determination of α_{eff} in addition to the strength of the external field. This phenomenon can be consistently explained by the reduced contribution from the small length-scale excitation and detection of the apparent dephasing or the spin-wave damping,[26] which comes from the inhomogeneous K_{eff} distribution, as witnessed in the domain evolution pattern in Fig. 1(c). This implies that the smaller beam spot pump-probe technique further mitigates the apparent dephasing or the additional spin-wave damping.

It has been reported that α has a proportional relationship with PMA in Co/Pd and Co/Pt systems.[4,5] In these systems, spin pumping causes by the Pt or Pd layers which have strong spin orbit coupling and d-d hybridization occurs at the Co atomic layer in contact with the Pd or Pt layer. Contrary to the interfacial spin pumping effect, the α in our experiment is not inversely proportional to the ferromagnetic layer thickness, as shown in Fig. 3(a). Also, the spin-orbit coupling constant of Ti is more than 10 times weaker than that of Pd or Pt. Therefore, we believed that the spin-pumping effect is negligible in our system. The 3d-3d hybridization is much weaker than 3d-4d(5d) hybridization.[27] In addition, PMA is caused by not only magnetocrystalline anisotropy but also shape anisotropy which arises from the dipole-dipole interaction in Co based multilayer system.[28] Therefore, there is no noticeable correlation between the PMA and the intrinsic α in our samples. Also, we could not find any noticeable relationship between the intrinsic α and the sample properties such as N and magnetic inhomogeneity. This indicates that the intrinsic α is well determined by the average damping of the atoms and layers, where the spins are coupled by strong exchange interactions and precessing in unison. Therefore, the highly local characteristic mainly contributes to the intrinsic α in this system.[6]

In conclusion, we systematically studied the Gilbert damping constant in relation to the stack number and the PMA by using an all-optical method with varying the external magnetic field strength and the angle as well as the pump-probe beam size. In our Ti-buffered Co/Ni multilayer system, the intrinsic Gilbert damping constant was found to be independent of the PMA and the stack number. We also noted that the magnetic inhomogeneity significantly affects the Gilbert damping constant as the extrinsic effect in a low external magnetic field. Intriguingly, the effect of the apparent dephasing or the additional spin-wave damping was shown to be mitigated with the decreasing length scale in the excitation and detection measurements of the all-optical method.

This work was supported by the NRF funds (Grant Nos. R0A-2007-000-200226-0, 2010-0023798, and 2010-0022040) of the Ministry of Education, Science and Technology of Korea. It was also supported by the DGIST R&D Program of the Ministry of Education, Science and Technology of Korea (11-IT-01).

[1]D. Lacour, J. A. Katine, N. Smith, M. J. Carey, and J. R. Childress, Appl. Phys. Lett. **85**, 4681 (2004).
[2]V. Kamberský, Phys. Rev. B **76**, 134416 (2007).
[3]K. Gilmore, Y. U. Idzerda, and M. D. Stiles, J. Appl. Phys. **103**, 07D303 (2008).
[4]S. Mizukami, E. P. Sajitha, D. Watanabe, F. Wu, T. Miyazaki, H. Naganuma, M. Oogane, and Y. Ando, Appl. Phys. Lett. **96**, 152502 (2010).
[5]S. Pal, B. Rana, O. Hellwig, T. Thomson, and A. Barman, Appl. Phys. Lett. **98**, 082501 (2011).
[6]J. M. Shaw, H. T. Nembach, and T. J. Silva, Appl. Phys. Lett. **99**, 012503 (2011).

[7]J. Shaw, H. Nembach, and T. Silva, Phys. Rev. B **85**, 054412 (2012).
[8]A. Barman, S. Wang, O. Hellwig, A. Berger, E. E. Fullerton, and H. Schmidt, J. Appl. Phys. **101**, 09D102 (2007).
[9]T. Kato, Y. Matsumoto, S. Okamoto, N. Kikuchi, O. Kitakami, N. Nishizawa, S. Tsunashima, and S. Iwata, IEEE Trans. Magn. **47**, 3036 (2011).
[10]S. Mizukami, X. Zhang, T. Kubota, H. Naganuma, M. Oogane, Y. Ando, and T. Miyazaki, Appl. Phys. Express **4**, 013005 (2011).
[11]J. Walowski, M. D. Kaufmann, B. Lenk, C. Hamann, J. McCord, and M. Münzenberg, J. Phys. D **41**, 164016 (2008).
[12]S. Mangin, D. Ravelosona, J. A. Katine, M. J. Carey, B. D. Terris, and E. E. Fullerton, Nat. Mater. **5**, 210 (2006).
[13]S.-B. Choe, D.-H. Kim, Y.-C. Cho, H.-J. Jang, K.-S. Ryu, H.-S. Lee, and S.-C. Shin, Rev. Sci. Instrum. **73**, 2910 (2002).
[14]D.-H. Kim, S.-B. Choe, and S.-C. Shin, Phys. Rev. Lett. **90**, 087203 (2003).
[15]S.-B. Choe and S.-C. Shin, IEEE Trans. Magn. **36**, 3167 (2000).
[16]K.-D. Lee, K.-S. Ryu, J.-W. Kim, H.-S. Song, J.-W. Jeong, and S.-C. Shin, Phys. Rev. B **82**, 140401(R) (2010).
[17]E. Beaurepaire, J. C. Merle, A. Daunois, and J. Y. Bigot, Phys. Rev. Lett. **76**, 4250 (1996).
[18]T. Ogasawara, K. Ohgushi, Y. Tomioka, K. Takahashi, H. Okamoto, M. Kawasaki, and Y. Tokura, Phys. Rev. Lett. **94**, 087202 (2005).
[19]S. Mizukami, S. Iihama, N. Inami, T. Hiratsuka, G. Kim, H. Naganuma, M. Oogane, and Y. Ando, Appl. Phys. Lett. **98**, 052501 (2011).
[20]H. Stillrich, C. Menk, R. Froümter, and H. P. Oepen, J. Appl. Phys. **105**, 07C308 (2009).
[21]W. Platow, A. Anisimov, G. Dunifer, M. Farle, and K. Baberschke, Phys. Rev. B **58**, 5611 (1998).
[22]S. Mizukami, D. Watanabe, T. Kubota, X. Zhang, H. Naganuma, M. Oogane, Y. Ando, and T. Miyazaki, Appl. Phys. Express **3**, 123001 (2010).
[23]G. Malinowski, K. C. Kuiper, R. Lavrijsen, H. J. M. Swagten, and B. Koopmans, Appl. Phys. Lett. **94**, 102501 (2009).
[24]S. Serrano-Guisan, K. Rott, G. Reiss, and H. W. Schumacher, J. Phys. D **41**, 164015 (2008).
[25]See supplementary material at http://dx.doi.org/10.1063/1.4795013 for the Gilbert damping constant dependences on the magnetization tilt angle.
[26]H. Suhl, IEEE Trans. Magn. **34**, 1834 (1998).
[27]P. H. Dederichs, R. Zeller, H. Akai, and H. Ebert, J. Magn. Magn. Mater. **100**, 241 (1991).
[28]M. T. Johnson, P. J. H. Bloemen, F. J. A. den Broeder, and J. J. de Vries, Rep. Prog. Phys. **59**, 1409 (1996).